JOURNAL OF Materials CHEMISTRY

Metal-rich polyantimonides: internal competition between M–M and Sb–Sb and heteroatomic M–Sb interactions in $(Zr,V)_{13}Sb_{10}$ and $(Zr,V)_{11}Sb_8$ (M = Zr,V)

Holger Kleinke

FB Chemie-Wissenschaftliches Zentrum für Materialwissenschaften, Philipps-Universität Marburg, Hans-Meerwein-Straße, D-35032 Marburg, Germany.
E-mail: kleinke@mailer.uni-marburg.de

Received 5th May 1999, Accepted 6th July 1999

The title compounds are accessible by arc-melting of suitable mixtures of Zr, V and $ZrSb_2$. Their crystal structures were determined *via* single crystal measurements on an IPDS diffractometer. Depending on the M : Sb ratio (M = Zr, V; M : Sb = 13 : 10 or 11 : 8), the phases crystallize in two related structure types, namely $Zr_{7.5}V_{5.5}Sb_{10}$ and $Cr_{11}Ge_8$. The lattice dimensions of $Zr_{7.46(5)}V_{3.54}Sb_8$ are $a = 1514.7(1)$, $b = 570.77(5)$, $c = 1811.1(2)$ pm, $V = 1565.8(2) \times 10^6$ pm^3 (*Pnma*, $Z = 4$). The structures may be considered as intergrowths of (distorted) fragments of the W_5Si_3 and NiAs structure types. In addition to M–Sb and homonuclear (and heteronuclear) M–M bonds, Sb–Sb bonding interactions, with Sb–Sb distances shorter than in elemental antimony, occur in the linear Sb chains of the W_5Si_3-analogous structural motifs. The entropy-stabilized phases decompose by annealing at lower temperatures. The metallic character was confirmed *via* extended Hückel calculations as well as measurements of the electrical resistivities.

Introduction

Within the last few years, a multitude of new metal-rich refractory pnictides and chalcogenides (M_xQ, M/Q ratio >1) of the valence-electron-poor transition metals have been uncovered, which formed hitherto unknown structure types in most cases. Recent examples include Sc_2Te,[1] Sc_8Te_3 and Y_8Te_3,[2] Ti_9Se_2,[3] $Ti_{11}Se_4$,[4] Zr_2Te,[5] Hf_7P_4,[6] Hf_2Te,[7] Hf_3Te_2,[8] Ta_3S_2,[9] Ta_2Se,[10] dd-$Ta_{1.6}Te$[11] and Ta_6Te_5.[12] Although these compounds differ significantly in their structures (*e.g.* two- and three-dimensional, crystalline and quasi-crystalline) as well as in their physical properties (*e.g.* metallic and non-metallic), they can be divided into two structural classes. The division into classes is based on differences in the metal atom substructure, which contains either extended fragments of the bcc packing type or icosahedral fragments. The antimonides Zr_2Sb,[13] Zr_5Sb_3,[14] Hf_5Sb_3,[15] Hf_6TiSb_4[16] and V_3Sb_2[17] stand out of this group in that they belong to neither of these classes. Only the latter two compounds are in part stabilized by Q–Q bonding interactions, whereas the structures of all the examples given exhibit M–M and M–Q bonding. In general, the occurrence of weak Sb–Sb bonding ($d_{Sb-Sb} > 320$ pm) is understandable because antimony is the most electropositive of the Q elements above, and thus possibly the least reduced one.

Here, two antimonides are introduced whose structures form a new family, containing linear Sb chains with Sb–Sb separations shorter than the shortest bonds in elemental antimony. The least metal-rich one, $(Zr,V)_{13}Sb_{10}$, was recently discussed in a short communication,[18] while $(Zr,V)_{11}Sb_8$ is presented here for the first time. The structural relations, Sb–Sb bonding and physical properties will be discussed in this article.

Experimental section

Synthesis

For the synthesis of the title compounds, $ZrSb_2$ was prepared first in a sealed silica tube at 650 °C over a period of five days, starting from the elements in the stoichiometric ratio 1 : 2 (Zr: ALFA, powder, 4–20 mesh, 99.6%; Sb: MERCK, powdered, >99%). The ternary antimonides $(Zr,V)_{13}Sb_{10}$ and $(Zr,V)_{11}Sb_8$ were synthesized by arc-melting in an argon atmosphere of corresponding mixtures of Zr, V (ABCR, powder, 45 micron, 99.7%) and $ZrSb_2$. An excess of 6–8% antimony was added to compensate for weight loss due to vaporization. The compounds formed needle-like crystals. Alternative routes to either $(Zr,V)_{13}Sb_{10}$ or $(Zr,V)_{11}Sb_8$ at temperatures below 1350 °C failed; annealing of these phases at 1100 °C resulted in their decomposition into mixtures of $Zr_2V_6Sb_8$,[19] Zr_5VSb_3,[20] ZrSb[21] and, to a small extent, other unidentified products.

No impurities were detected during energy dispersive X-ray analyses, performed using an electron microscope (CAM-SCAN, CS 4DV) with an additional EDX device (detector: NORAN Instruments) on selected crystals. Based on Guinier diagrams and (standardless) EDX results, a certain phase range exists in the case of $(Zr,V)_{13}Sb_{10}$ with Zr : V ratios between 7.5 : 5.5 and 5 : 8, while no noticeable phase range was detected in the case of $(Zr,V)_{11}Sb_8$.

Structure determination

Single crystal structure studies were performed on needle-like crystals using an IPDS diffractometer (STOE). The structure solution was carried out based on direct methods using SHELXS-86.[22] The refinements were done with SHELXL-97.[23] In the first step, all nine metal sites were refined as being occupied with mixed Zr and V atoms. Within the standard deviations, five sites were refined to be occupied solely by Zr atoms, while two pure V sites resulted. The eighth position (M1) was found to be occupied by a mixture of 87(3)% Zr and 13% V, and the ninth (M2) by 79.5(1.5)% Zr and 20.5% V. The introduction of these mixed occupancies led to an improvement of the final $R(F)$ value from 3.24% to 3.14%, while the data : parameter ratio decreased from 1322 : 107 to 1322 : 109. The probability of a significant improvement is thus higher than 99.5% according to the Hamilton test.[24] In general, uniform displacement parameters were found, with the exceptions of the V1, M1 and Sb5 atoms. These atoms are all interconnected *via* short bonds, *i.e.* the anisotropies are likely to have an impact from one site to the other. The

peculiarities of the V1 and M1 atoms are discussed in the following chapter. Details of the hitherto unpublished structure study on $(Zr,V)_{11}Sb_8$ are summarized in Table 1, atomic coordinates, equivalent displacement parameters, and occupancy factors are listed in Table 2.

Full crystallographic details, excluding structure factor tables have been deposited at the Cambridge Crystallographic Data Centre (CCDC). Any request to the CCDC for this materal should quote the full literature citation and the reference number 1145/169. See http://www.rsc.org/suppdata/jm/1999/2703 for crystallographic files in .cif format.

The refined formula of $Zr_{7.46(5)}V_{3.54}Sb_8$ is in good agreement with the starting Zr : V ratio of 2. Arc-melting the elements in the stoichiometric ratio Zr : V : Sb = 7.5 : 3.5 : 8 in an attempt to reproduce $Zr_{7.5}V_{3.5}Sb_8$ (with an excess of 8% Sb to compensate for the weight loss during the process of arc-melting) led to the formation of $(Zr,V)_{11}Sb_8$ in quantitative yields.

Calculation of the electronic structure

Semiempirical calculations were performed using the extended Hückel approximation.[25–27] The Hückel parameters were taken from calculations on $Zr_2V_6Sb_9$.[19] Three different structural models were used, since mixed occupancies cannot be handled within the Hückel theory. For calculations on $(Zr,V)_{13}Sb_{10}$, the positional parameters were taken from the single crystal study on $Zr_{7.5}V_{5.5}Sb_{10}$, while the atoms were assigned according to the predominating atom in each position. This results in the formula $Zr_7V_6Sb_{10}$; the M atoms of the NiAs-like fragments were considered as V, and those of the W_5Si_3-like fragments as Zr. Following the same criterion, the electronic structure of $Zr_{7.5}V_{3.5}Sb_8$ was estimated by calculation of a structural model with Zr parameters for the M1 and M2 sites, which show a 13–20% incorporation of vanadium, leading to the hypothetical formula $Zr_8V_3Sb_8$.

In addition, the band structure of the structural model $^1_\infty[Zr_7Sb_2]$, with the positional parameters taken from $Zr_{7.5}V_{5.5}Sb_{10}$, was calculated in order to model the Sb substructure.

Table 1 Crystallographic data for $(Zr,V)_{11}Sb_8$

Chemical formula: $Zr_{7.46(5)}V_{3.54}Sb_8$	Formula weight: 1834.83
$a = 1514.7(1)$ pm	Space group: *Pnma* (No. 62)
$b = 570.77(5)$ pm	$T = 22$ °C
$c = 1811.1(2)$ pm	$\lambda = 71.069$ pm
$V = 1565.8(2) \times 10^6$ pm^3	$\rho_{calc} = 7.78$ g cm^{-3}
No. of reflections: 13193	Unique reflections: 2063 ($R_{int} = 0.071$)
$Z = 4$	$R(F_o)^a = 0.031$; $R_w(F_o^2)^b = 0.065$

$^aR(F_o) = \Sigma||F_o| - |F_c||/\Sigma|F_o|$.
$^bR_w(F_o^2) = \{\Sigma[w(F_o^2 - F_c^2)^2]/\Sigma[w(F_o^2)^2]\}^{1/2}$.

Physical properties

Temperature dependent resistivity measurements down to 10 K were performed on a cold-pressed bar as well as on a needle-like single crystal of a sample wth the nominal composition $Zr_{6.5}V_{6.5}Sb_{10}$ ($Zr_{7.5}V_{5.5}Sb_{10}$ structure type). While the bar was contacted at four points, which enables a measurement independent of the resistivities of the contacts, the single crystal was contacted at two points only, due to its small length. The dimensions (in mm) were estimated under an optical microscope to be $3 \times 2 \times 1.5$ (bar) and $0.2 \times 0.015 \times 0.015$ (crystal).

Results and discussion

Entropy stabilization

Despite the relatively large differences between zirconium and vanadium, the metal positions are in part statistically occupied by mixtures of Zr and V atoms, leading to an increase in the configurational entropies. This is true for the three cases, $Zr_{7.5}V_{5.5}Sb_{10}$, $Zr_{6.5}V_{6.5}Sb_{10}$ and $Zr_{7.5}V_{3.5}Sb_8$, where single crystal studies were performed. Correspondingly, annealing at a temperature of 1100 °C over a period of five days under an argon atmosphere resulted in decomposition of these phases, because then the entropy contribution to the free enthalpy, $\Delta G = \Delta H - T\Delta S$, is not as important as it is at the higher temperatures reached in the arc-melter.

$Zr_{7.5}V_{5.5}Sb_{10}$, $Zr_{6.5}V_{6.5}Sb_{10}$ and $Zr_{7.5}V_{3.5}Sb_8$ are DFSO-stabilized materials, *i.e.* differential fractional site occupancies significantly enhance the stability of the compounds. The DFSO concept was introduced by Franzen *et al.*[28,29] The three criteria postulated for ternary DFSO-stabilized materials are as follows: (i) each metal atom site is mixed occupied by a mixture of two different metal atoms without long-range order, (ii) the fractional site occupancies, being more or less fixed per site, differ from one site to another, and (iii) their crystal structure types are not found in the binary systems. The first phases classified as DFSO-stabilized materials were the ternary niobium tantalum sulfides $Nb_{1.72}Ta_{3.28}S_2$,[30] $Nb_{1.90}Ta_{2.10}S_2$,[31] $Nb_{4.92}Ta_{6.08}S_4$[32] and $Nb_{6.74}Ta_{5.26}S_4$,[33] whose structures are unknown among the binary niobium sulfides as well as among the binary tantalum sulfides. To date, two other examples containing metal atoms from groups 4 and 5 have been described, namely $Zr_{6.45}Nb_{4.55}P_4$[34] and $(Hf,Nb)_{10}Ni_3P_5$.[35] In these two cases, as well as in the structures discussed in this article, not all metal sites exhibit mixed occupancies, which is a consequence of the larger differences between the metal atom

Table 2 Atomic positions, equivalent displacement parameters and occupancy factors for $Zr_{7.5}V_{3.5}Sb_8$

Site	x	y	z	U_{eq}/pm^2	Occupancy
Zr1	0.4345(1)	1/4	0.19290(8)	92(3)	1
Zr2	0.1283(1)	1/4	0.04275(8)	74(3)	1
Zr3	0.1951(1)	1/4	0.74861(9)	102(3)	1
Zr4	0.3658(1)	1/4	0.66247(9)	108(3)	1
Zr5	0.2526(1)	1/4	0.46573(9)	91(3)	1
V1	0.0481(2)	1/4	0.5888(2)	273(8)	1
V2	0.3614(1)	0.0182(3)	0.82379(9)	74(4)	1
M1	0.3886(1)	1/4	0.9906(1)	232(8)	87(3)% Zr + 13%V
M2	0.06014(7)	0.0018(2)	0.87519(6)	86(4)	79.5(1.5)%Zr + 20.5%V
Sb1	0.29051(7)	1/4	0.30084(6)	83(2)	1
Sb2	0.44222(7)	1/4	0.51715(6)	83(2)	1
Sb3	0.08744(7)	1/4	0.20080(6)	80(2)	1
Sb4	0.22917(7)	1/4	0.90573(6)	91(2)	1
Sb5	0.00885(8)	1/4	0.73111(8)	208(3)	1
Sb6	0.05787(8)	1/4	0.43451(6)	161(3)	1
Sb7	0.28928(5)	0.0023(2)	0.10699(4)	154(2)	1

pairs Zr and Nb, Zr and V, and Hf and Nb, as compared to Nb and Ta.

Crystal structure

While $(Zr,V)_{13}Sb_{10}$ crystallizes in its own structure type, $(Zr,V)_{11}Sb_8$ occurs in the $Cr_{11}Ge_8$[36] type. A projection along the short *b* axis of the structure of $(Zr,V)_{11}Sb_8$ is shown in Fig. 1. Formally, the structure consists, like the $(Zr,V)_{13}Sb_{10}$ structure (Fig. 2), of two distinct structural motifs, namely of fragments of the NiAs type and of the W_5Si_3 type. The metal atoms M^1, which are part of the latter motif, are shown as white circles, including the atoms Zr1–Zr5, V1 and M1. The two metal sites of the NiAs-like fragments (M^2: V2 and M2) are represented by black circles. However, the mnemonically useful concept of dividing these structures into fragments of the NiAs and W_5Si_3 types should not be pushed too far, because the fragments are interconnected *via* a multitude of metal–metal and metal–antimony bonds.

The Sb centered columns of the M^1 atoms are stacked like densely packed rods, a formation which can be described as 3^6 nets. On the other hand, the secondary tiling of these columns

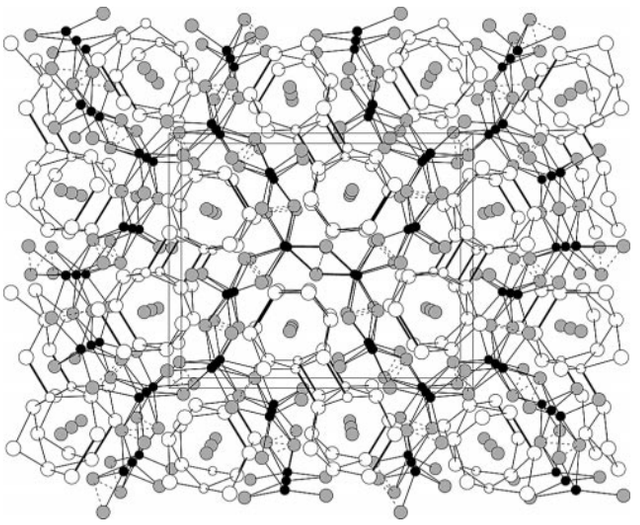

Fig. 1 Projection of the structure of $(Zr,V)_{11}Sb_8$ along [010]. Horizontal: *c* axis. White circles: M^1 (small: V1); black: M^2; gray: Sb.

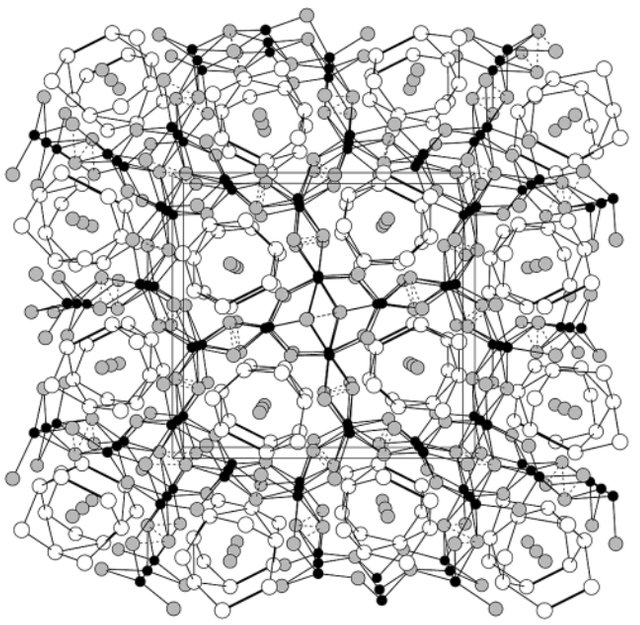

Fig. 2 Projection of the structure of $(Zr,V)_{13}Sb_{10}$ along [010]. Horizontal: *a* axis. White circles: M^1; black: M^2; gray: Sb.

in the structure of $(Zr,V)_{13}Sb_{10}$ is based on the semi-regular quadratic-triangular 3^2434 tiling. One further striking difference between the structures of $(Zr,V)_{13}Sb_{10}$ and $(Zr,V)_{11}Sb_8$ is found in the connection of two of these chains in $(Zr,V)_{11}Sb_8$ to a double chain *via* M^1–M^1 bonds, which expresses itself in the higher M : Sb ratio, and in particular in the higher Zr content, since Zr is predominant in the M^1 sites.

The different Zr/V occupancies of the different sites are attributed to size effects. The single bond radius of a Zr atom is almost 20% larger than that of a V atom (according to Pauling: 145 pm *vs.* 122 pm[37]), a fact which is reflected in the tendency of the Zr atoms to prefer the sites with higher coordination numbers and larger contacts to neighboring atoms. Also, the differences in metal–metal bonding per site play an important role because of the differences in electronegativity as well as in valence-electron numbers of Zr and V. Thus, one can only compare strongly related atom sites in order to get clear trends. Accordingly, considering the M^1 and M^2 positions separately gives the postulated tendencies in the cases of all three compounds examined, namely $Zr_{7.5}V_{5.5}Sb_{10}$, $Zr_{6.5}V_{6.5}Sb_{10}$, and $Zr_{7.5}V_{3.5}Sb_8$: the Zr content increases with decreasing bond order per site, as depicted in Fig. 3. Therein, the total Pauling bond order per M site (PBO) is used as a combined measure for both the coordination number and the bonds to the neighboring Sb atoms, which predominate the first coordination sphere. Pauling's equation [$d(n)=d(1)-(60\text{ pm}\times\log n)$, with $n=$bond order, $r_{Sb}=139$ pm] was used for the calculation of the PBOs, while the radius of the M^1 atoms was taken as $r_{Zr}=145$ pm and that of the M^2 atoms as $r_V=122$ pm.

The different columnar structural motifs of $(Zr,V)_{11}Sb_8$ are revealed in Fig. 4. The $^1_\infty[M^1{}_7Sb_2]_2$ chain is shown in the left part, while a part of the NiAs type fragment is shown on the right. Therein, the V2 and M2 atoms are located in Sb_6 and $Sb_5\square_1$ octahedra, respectively ($\square$ = vacancy). The M–Sb bond lengths of 278–307 pm are slightly larger than the sum of the radii of the constituent atoms. The octahedra are interconnected *via* common faces along the *b* axis and *via* common edges perpendicular to the *b* axis. Linear chains of V2 and M2 atoms run parallel to *b*, with the interatomic distances alternating between 265 and 306 pm (V2) and 283 and 287 pm (M2), respectively; the average of these distances is $b/2=285$ pm by symmetry. Two effects contribute to the different deviations from that mean distance: first, the irregularity of the $V2Sb_5$ coordination polyhedra expresses itself in an elongation of the V–V bond which is surrounded by three Sb atoms, compared to the shorter bond which is situated between two Sb atoms; and second, the high Zr content of 80% in the M2 position militates against formation of a bond significantly smaller than $b/2=285$ pm because of steric effects

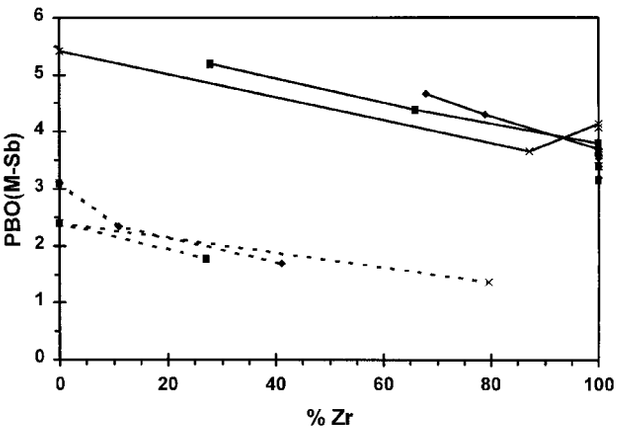

Fig. 3 Total M–Sb Pauling bond orders *vs.* % Zr occupancy per M site. ◆: $Zr_{7.5}V_{5.5}Sb_{10}$, ■: $Zr_{6.5}V_{6.5}Sb_{10}$, ×: $Zr_{7.5}V_{3.5}Sb_8$. Solid lines: M^1; dashed: M^2.

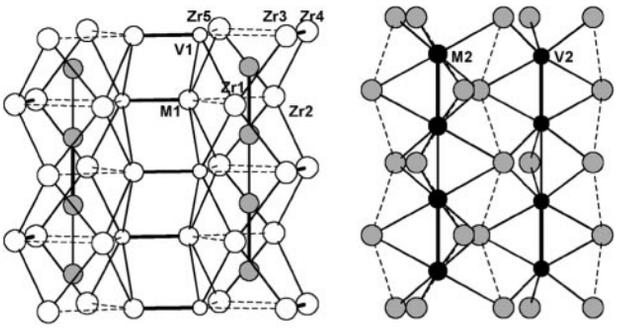

Fig. 4 Columnar structural motifs of $Zr_{7.5}V_{3.5}Sb_8$. Left: part of the $^1_\infty[M^1{}_7Sb_2]_2$ chain; right: part of the NiAs-like fragment.

$(2 \times r_{Zr} = 290$ pm). The V2–V2 bond of 265 pm is still significantly larger than twice the radius of V ($2 \times r_V = 244$ pm).

The Sb7 atom is coordinated by seven M^1 atoms, which form a defect square antiprism $M^1{}_7\square_1$. These antiprisms share common faces resulting in a linear chain of Sb7 atoms with alternating Sb–Sb bonds of 283 and 288 pm. The shorter bond is surrounded by three M1 atoms, and the longer by four, a situation which resembles that of the V2–V2 bonds. These Sb–Sb bonds are shorter than the shortest bond in elemental antimony, 291 pm, and compare well with the lengths of Sb–Sb single bonds. Examples can be found in the structures of KSb (283 and 285 pm),[38] *cyclo*-Sb_5^{5-} (between 281 and 291 pm)[39] and Sb_{11}^{3-} (between 276 and 285 pm).[40] However, the linearity of the Sb chain militates against 2-electron–2-center bonds, as comparisons with the zigzag Sb(–1) chains in KSb or the Te chains in elemental tellurium demonstrate.

Other Sb–Sb contacts in the structure of $(Zr,V)_{11}Sb_8$ occur in the NiAs-like units with lengths of 341–344 pm, *i.e.* of the order of the longest bond in elemental antimony (335 pm), which may hint at weak bonding interactions.

The Sb atoms surrounding the $^1_\infty[M^1{}_7Sb_2]_2$ unit are omitted for the sake of clarity. The Zr atoms Zr1, Zr2 and Zr5 are surrounded by seven Sb atoms forming a severely distorted pentagonal bipyramid, while the Zr3, Zr4, M1 and V1 sites are coordinated by six Sb atoms each. The $M1Sb_6$ and $V1Sb_6$ polyhedra are best described as metal-centered Sb octahedra, and the $Zr3Sb_6$ and $Zr4Sb_6$ polyhedra can be regarded as centered pentagonal pyramids. The shortest interatomic distance here is the V1–Sb5 bond of 265 pm, which is 13 pm shorter than the shortest V2–Sb bond.

Among the M^1 atoms, the lower coordination numbers (c.n.) correlate with the lengths of the metal–metal bonds: the shortest M–M distances involving Zr1, Zr2 and Zr5 (c.n. = 7) are as long as 343 pm, whereas Zr3 and Zr4 (c.n. = 6) are interconnected *via* a bond of 302 pm and also M1 and V1 (c.n. = 6) *via* a bond of 281 pm.

All of these observations, with the exceptions of the M1 and V1 sites, are principally transferable to the structure of $(Zr,V)_{13}Sb_{10}$, a fact which underlines the structural relations between $(Zr,V)_{13}Sb_{10}$ and $(Zr,V)_{11}Sb_8$.

Electronic structure

The densities of states of $(Zr,V)_{11}Sb_8$ and $(Zr,V)_{13}Sb_{10}$ are presented in Fig. 5. Principally, both DOS curves exhibit the same features. The peak at lower energies is predominantly due to the 5p states of antimony, while covalent mixing with the Zr and V atoms leads to some Zr and V contributions to this peak. This Sb peak overlaps only to a negligible extent with the partly occupied conduction band, which consists mainly of Zr and V states, while the V contributions occur on average at lower energies. The Fermi level falls in either case into a region with a high density of states, although being close to a local minimum. Therefore, metallic properties are to be expected, independent of the exact Zr : V ratio of the phases. Furthermore, the

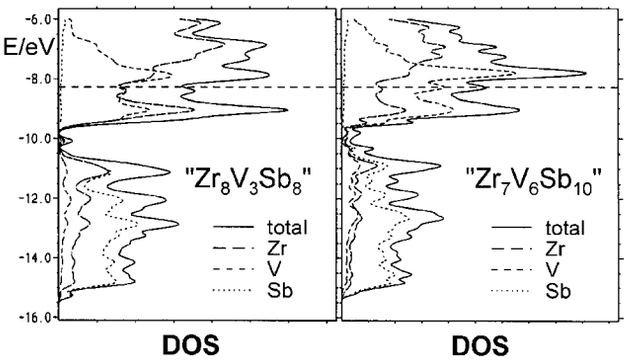

Fig. 5 Densities of states. Left: '$Zr_8V_3Sb_8$'; right: '$Zr_7V_6Sb_{10}$'. Dashed, horizontal lines: Fermi levels. Solid line: total DOS; long dashes: Zr; short dashes: V; dotted: Sb contributions.

densities of states at the Fermi level are comparable, strongly suggesting similar metallic character in $(Zr,V)_{13}Sb_{10}$ and $(Zr,V)_{11}Sb_8$. The main difference between the two DOS curves shown lies in the ratios of the Zr and V peaks and is therefore a consequence of the differences in the stoichiometry of the structure models $Zr_8V_3Sb_8$ and $Zr_7V_6Sb_{10}$.

Selected crystal orbital overlap populations (COOP curves) of the structure models $Zr_8V_3Sb_8$ and $Zr_7V_6Sb_{10}$ are depicted in the Fig. 6 and 7. Overall, strong bonding interactions are calculated in both cases for all three kinds of metal–metal contacts, namely Zr–Zr, V–V as well as Zr–V. While the Zr–V interactions are optimized at the Fermi level, increasing the valence-electron numbers (and thus raising the Fermi level) would lead to weaker V–V bonds by filling antibonding states, but stronger Zr–Zr bonds by filling more bonding states.

Since an electron transfer from a metal atom to an Sb atom is likely to happen, most of the Sb states are filled at the Fermi level in both structure models. This assumption, which is supported by the DOS curves shown, is reflected by the occurrence of antibonding Sb–Sb states below the Fermi level. The net Mulliken overlap populations (MOP)[41] of the longer Sb–Sb distances (*ca.* 340 pm) are on average 0.02 electrons per bond. This value is smaller than the MOP of 0.08 for the 335 pm Sb–Sb bond in elemental antimony. However, the small, but positive values support the supposition of weak bonding, which was also found for even longer distances: *ab initio* calculations suggested an Sb–Sb attraction due to correlation effects in the dipnictogen hydride model dimer $(H_2Sb–SbH_2)_2$, which has an Sb–Sb distance of 378.5 pm.[42] This is supported by measurements of the force constant ($0.125\ N\ cm^{-1}$) of the intermolecular Sb–Sb interaction (368 pm) in $Sb_2(CH_3)_4$. This is more than 10% of the value for the intramolecular interaction of 284 pm ($1.1\ N\ cm^{-1}$).[43]

In the cases of the Sb–Sb bonds which are shorter than

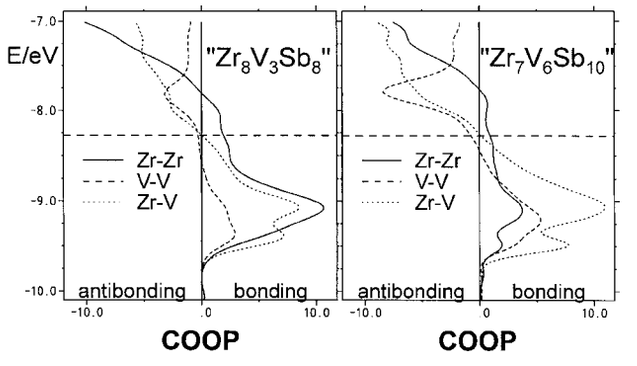

Fig. 6 Summed COOP curves. Left: '$Zr_8V_3Sb_8$'; right: '$Zr_7V_6Sb_{10}$'. Dashed, horizontal lines: Fermi levels. Solid line: Zr–Zr; dashed: V–V; dotted: Zr–V interactions. Right parts of the diagrams: bonding (+), left parts: antibonding interactions (−).

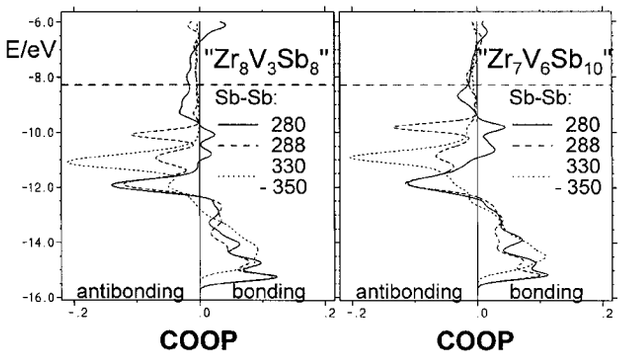

Fig. 7 Averaged COOP curves. Left: '$Zr_8V_3Sb_8$'; right: '$Zr_7V_6Sb_{10}$'. Dashed, horizontal lines: Fermi levels. Solid lines: Sb–Sb distances $\approx$280 pm; dashed: $d_{Sb-Sb} \approx 288$ pm, dotted: 330 pm $< d_{Sb-Sb} <$ 350 pm. Right parts of the diagrams: bonding (+), left parts: antibonding interactions (−).

290 pm (located in the linear Sb chains), the filled bonding states by far outweigh the antibonding contributions, resulting in larger positive MOPs of 0.39 (d = 283 pm) and 0.28 (288 pm) for $Zr_8V_3Sb_8$ and similar values for $Zr_7V_6Sb_{10}$ (0.45–0.26). The large differences between the shorter and the longer bonds in the linear Sb chains stem from bonding contributions between −11 and −9.5 eV in the case of the shorter bonds, while in the case of the longer bonds antibonding states are occupied in this energy region. The MOP of a typical Sb–Sb single bond (*e.g.* 0.65 in KSb)[44] is almost twice that of the values calculated for the Sb–Sb bonds in the linear $^1_\infty[M^1{}_7Sb_2]_2$ units (average 0.35), while the distances are comparable.

In order to gain some insight into the bonding in the Sb chain, the schematic band structure of an infinite Zr_7Sb_2 chain is shown in Fig. 8. The s_σ, s_σ*, p_π, p_π* and p_σ bands of the two Sb atoms are all completely filled, occurring well below the Zr centered states. Since the p_π bands stem from both the p_x and the p_z orbitals (p_y is parallel to the chain direction), seven bands of the two Sb atoms of the unit are completely filled, *i.e.* with two electrons per band. One can therefore consider these Sb atoms as Sb(−2), forming (delocalized) 1-electron–2-center σ Sb–Sb bonds. This is in agreement with the values of the overlap populations as discussed above. The mismatch of bond length and bond strength is thought to arise from matrix effects, enabling a relatively short b axis and thus strongly bonding metal–metal interactions parallel to the b axis as well as regular M^1–Sb bonds within the $^1_\infty[M^1{}_7Sb_2]_2$ units.

In contrast to the Sb atoms of the $^1_\infty[M^1{}_7Sb_2]_2$ motifs, the other Sb atoms can be regarded as Sb(−3), ignoring to a first approximation the Sb–Sb contacts of *ca.* 340 pm. The higher oxidation states express themselves in higher Mulliken gross populations, which range in the case of $Zr_8V_3Sb_8$ from 5.41 to 5.58 (Sb1–Sb6), while the Mulliken population of Sb7 (5.06) is significantly smaller. Basically the same differences were found

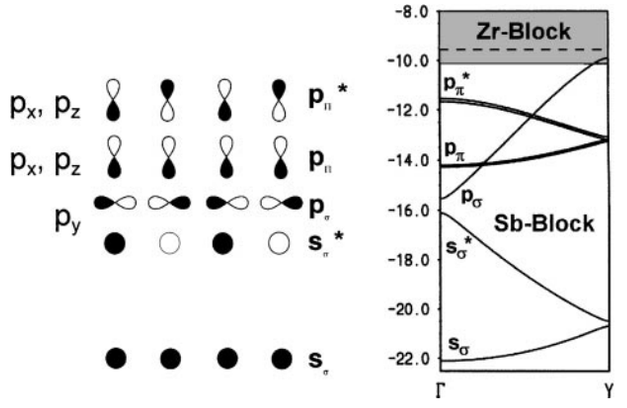

Fig. 8 Schematic band structure of a $^1_\infty[Zr_7Sb_2]$ unit.

in the case of $Zr_7V_6Sb_{10}$ with gross populations of 5.07 for the Sb(−2) atom and 5.38–5.52 for the Sb(−3) atoms.

Physical properties

The measurements performed on $Zr_{6.5}V_{6.5}Sb_{10}$ as an example for the $(Zr,V)_{13}Sb_{10}$ phase confirm the suggestion of metallic properties, which was based on the calculations on the structure models $Zr_7V_6Sb_{10}$ and $Zr_8V_3Sb_8$. The electrical conductivity decreases smoothly from 10 to 300 K as is typical for metals, while the values of the specific resistivity at room temperature (bulk: 5.5 mΩ cm; crystal, measured parallel to [010]: 1.2 mΩ cm) classify the material as a poorly conducting metal. It should be noted that the absolute values of the specific resistivity might occur with an error of 200–300%, however, the magnitude is smaller by a factor of 10^4 than that of copper, a very good metallic conductor.

Acknowledgements

The financial support of the Deutsche Forschungsgemeinschaft, the Fonds der Chemischen Industrie and the Bundesministerium für Bildung, Wissenschaft, Forschung und Technologie is gratefully acknowledged. Insightful discussions with Professor Dr. B. Harbrecht are appreciated.

References

1 P. A. Maggard and J. D. Corbett, *Angew. Chem., Int. Ed. Engl.*, 1997, **36**, 1974.
2 P. A. Maggard and J. D. Corbett, *Inorg. Chem.*, 1998, **37**, 814.
3 T. E. Weirich, A. Simon and R. Pöttgen, *Z. Anorg. Allg. Chem.*, 1996, **622**, 630.
4 T. E. Weirich, R. Ramlau, A. Simon and S. Hovmöller, *Nature*, 1996, **382**, 144.
5 G. Örlygsson and B. Harbrecht, *Inorg. Chem.*, 1999, **38**, 3377.
6 H. Kleinke and H. F. Franzen, *Angew. Chem., Int. Ed. Engl.*, 1996, **35**, 1934.
7 B. Harbrecht, M. Conrad, T. Degen and R. Herbertz, *J. Alloys Compd.*, 1997, **255**, 178.
8 R. L. Abdon and T. Hughbanks, *Angew. Chem., Int. Ed. Engl.*, 1994, **33**, 2328.
9 S.-J. Kim, K. S. Nanjundaswamy and T. Hughbanks, *Inorg. Chem.*, 1991, **30**, 159.
10 B. Harbrecht, *Angew. Chem., Int. Ed. Engl.*, 1989, **28**, 1660.
11 M. Conrad, F. Krumeich and B. Harbrecht, *Angew. Chem., Int. Ed.*, 1998, **37**, 1383.
12 M. Conrad, Ph.D. thesis, University of Dortmund, Germany, 1997.
13 E. Garcia and J. D. Corbett, *J. Solid State Chem.*, 1988, **73**, 440.
14 E. Garcia and J. D. Corbett, *Inorg. Chem.*, 1988, **27**, 2353.
15 H. Kleinke and C. Felser, *J. Alloys Compd.,* in press.
16 H. Kleinke, *Inorg. Chem.*, 1999, **38**, 2931.
17 J. Steinmetz, B. Malaman and B. Roques, *C. R. Seances Acad. Sci., Ser. C*, 1977, **284**, 499.
18 H. Kleinke, *Chem. Commun.*, 1998, 2219.
19 H. Kleinke, *Eur. J. Inorg. Chem.*, 1998, 1369.
20 Zr_5VSb_3 was identified based on EDX investigations and a Guinier diagram by analogy to Zr_5ZSb_3 with Z = Fe, Co, Ni, *etc.*, see: E. Garcia, H. C. Ku, R. N. Shelton and J. D. Corbett, *Solid State Commun.*, 1988, **65**, 757.
21 E. Garcia and J. D. Corbett, *J. Solid State Chem.*, 1988, **73**, 452.
22 G. M. Sheldrick, SHELXS-86, University of Göttingen, Germany, 1986.
23 G. M. Sheldrick, SHELXL-97, University of Göttingen, Germany, 1997.
24 W. C. Hamilton, *Acta Crystallogr.*, 1965, **18**, 502.
25 R. Hoffmann, *J. Chem. Phys.*, 1963, **39**, 1397.
26 M.-H. Whangbo and R. Hoffmann, *J. Am. Chem. Soc.*, 1978, **100**, 6093.
27 Program EHMACC, adapted for use on a PC by M. Köckerling, Gesamthochschule Duisburg, Germany, 1997.
28 X. Yao, G. A. Marking and H. F. Franzen, *Ber. Bunsen-Ges. Phys. Chem.*, 1992, **96**, 1552.
29 H. F. Franzen and M. Köckerling, *Prog. Solid State Chem.*, 1995, **23**, 265.
30 X. Yao and H. F. Franzen, *J. Am. Chem. Soc.*, 1991, **113**, 1426.

31 X. Yao, G. J. Miller and H. F. Franzen, *J. Alloys Compd.*, 1992, **183**, 7.
32 X. Yao and H. F. Franzen, *J. Solid State Chem.*, 1990, **86**, 88.
33 X. Yao and H. F. Franzen, *Z. Anorg. Allg. Chem.*, 1991, **589/599**, 353.
34 G. A. Marking and H. F. Franzen, *Chem. Mater.*, 1993, **5**, 678.
35 H. Kleinke and H. F. Franzen, *J. Am. Chem. Soc.*, 1997, **119**, 12824.
36 P. Israiloff, H. Völlenke and A. Wittmann, *Monatsh. Chem.*, 1974, **105**, 1387.
37 L. Pauling, *The Nature of the Chemical Bond*, Cornell University Press, Ithaca, NY, 3rd edn., 1948.
38 W. Hönle and H.-G. von Schnering, *Z. Kristallogr.*, 1981, **155**, 307.
39 N. Korber and F. Richter, *Angew. Chem., Int. Ed. Engl.*, 1997, **36**, 1512.
40 U. Bolle and W. Tremel, *J. Chem. Soc., Chem. Commun.*, 1992, 91.
41 R. S. Mulliken, *J. Chem. Phys.*, 1955, **23**, 2343.
42 K. W. Klinkhammer and P. Pykkö, *Inorg. Chem.*, 1995, **34**, 4134.
43 H. Bürger, R. Eujen, G. Becker, O. Mundt, M. Westerhausen and C. Witthauer, *J. Mol. Struct.*, 1983, **98**, 265.
44 H. Kleinke, unpublished calculations.

Paper 9/03582F